*Int. J. Heat Mass Transfer.* Vol. 32, No. 11, pp. 2087–2098, 1989
Printed in Great Britain

0017–9310/89 $3.00 + 0.00


# Evolution of a binary system crystallizing in a confined region

A. M. LEITCH†
Department of Mechanical Engineering, University of Toronto, Toronto, Ontario, Canada M5S 1A4

(*Received* 5 *May* 1988 *and in final form* 8 *March* 1989)

**Abstract**—The time evolution of the mean properties of a binary system is studied as one component crystallizes at a constant temperature boundary from either a semi-infinite or a confined liquid. Regimes are identified where the evolution is controlled by convective transport from the liquid, conduction of heat through the crystals, or the limited resources of a confined system. For a confined liquid there are different time-scales for change of temperature and concentration. There is good agreement between the predictions of the equations and the results of experiments where a binary aqueous solution crystallizes at a side boundary. The experimentally determined Sherwood number is an order of magnitude greater than that for laminar convection from a flat wall, and this is attributed to the roughness of the crystal interface.

## 1. INTRODUCTION

RECENT interest in crystallization in confined systems has arisen from applications in geology and metallurgy. Crystallization at a boundary may provide a mechanism for the differentiation of magmas when they solidify in chambers in the earth's crust [1, 2], and also of binary alloys [3].

Investigations in this field have concentrated on crystallization from a single flat, vertical, horizontal or sloping boundary and have consisted of experimental observations of liquid differentiation in aqueous solutions [2, 4] or a mathematical treatment of a two-component boundary layer [5–7]. The present work gives a one-dimensional mathematical analysis of crystallization from a vertical wall. It aims at a quantitative description of the volume averaged properties of the system, without reference to the vertical differentiation of the liquid or the detailed structure of the boundary layer.

Figure 1 is a diagram of a typical experiment. The crystals grow outwards from the cold wall in a tightly packed aggregate with a surface roughness of a few millimeters. In the cold, depleted boundary layer the compositional effect on buoyancy dominated so there was upward flow and the tank became stratified from the top downwards as the boundary layer fluid was expelled into the environment. Because the most depleted fluid was also the coldest, the stratification, while stable in density was unstable with respect to temperature and the lower part of the compositionally stratified region broke up into double-diffusive layers. The emphasis of this paper is on changes in volume averaged properties only, and the purpose of describing the differentiated environment is to give a realistic impression of the system that is being modelled.

The laboratory system is not readily accessible to rigorous mathematical analysis. The following analysis calls upon only the basis laws of conservation, some simplifying assumptions are made and key parameters must be measured from the experiments. It has been found possible to produce a simple model of the evolution of the system, which is justified by its good agreement with the experiments.

## 2. EXPERIMENTS

The solute used in the experiments was sodium carbonate which forms a decahydrate crystal ($Na_2CO_3 \cdot 10H_2O$). It has a high solubility in water and the saturation concentration is a strong function of temperature (Fig. 7). The apparatus used is shown in Fig. 2. The experimental tank was made of plexiglass except for the cold wall which was a heat exchanger. The copper surface of the cold wall was scored diagonally at 1 mm intervals to provide easy sites for nucleation. The tank was insulated by 10 cm thick expanded polystyrene. Experiments were carried out for two different tank lengths and to change the length a 10 cm block of expanded polystyrene was inserted into the end of the tank.

Ethanol (50 l) was precooled to about $-18°C$ by an FTS FC40 refrigeration unit, and then circulated through the heat exchanger by a Braun 1480 Thermomix. The temperature of the cold wall was regulated at 0°C.

Two thermistors (Fenwell GB38P12) were tracked up and down through the solution to record the time-changing temperature profiles. Concentration profiles were determined by withdrawing samples of the solu-

† Present address: Minnesota Supercomputer Institute and Department of Geology and Geophysics, University of Minnesota, Minneapolis, MN 55415, U.S.A.

## NOMENCLATURE

| | |
|---|---|
| $c$ | specific heat [J kg$^{-1}$ °C$^{-1}$] |
| $C$ | concentration [kg m$^{-3}$] |
| $D$ | diffusivity of concentration [m$^2$ s$^{-1}$] |
| $e$ | roughness height [m] |
| $g$ | acceleration of gravity [m s$^{-2}$] |
| $h$ | $h_C+h_T$ |
| $h_C$ | $(\Lambda\rho_S/k_S H)(m/(C_S-C_X))D\,Sh$ |
| $h_T$ | $k_L\,Nu/k_S H$ |
| $H$ | height of reservoir [m] |
| $k$ | thermal conductivity [W m$^{-1}$ °C$^{-1}$] |
| $L$ | length of reservoir [m] |
| $Le$ | Lewis number, $\kappa/D$ |
| $Nu$ | Nusselt number, $(H/\Delta T)(\partial T_{LX}/\partial x)$ |
| $Pr$ | Prandtl number, $\nu/\kappa$ |
| $Ra_z$ | Rayleigh number, $g\alpha\Delta T z^3/\nu\kappa$ |
| $Rs_z$ | compositional $Ra$, $g\beta\Delta C z^3/\nu D$ |
| $Sh$ | Sherwood number, $(H/\Delta C)(\partial C_{LX}/\partial x)$ |
| $t$ | time [s] |
| $T$ | temperature [°C] |
| $x$ | horizontal distance [m] |
| $X$ | position of interface [m] |
| $z$ | vertical distance [m]. |

Greek symbols

| | |
|---|---|
| $\alpha$ | coefficient of thermal expansion [°C$^{-1}$] |
| $\beta$ | compositional equivalent of $\alpha$ [m$^3$ kg$^{-1}$] |
| $\kappa$ | thermal diffusivity [m$^2$ s$^{-1}$] |
| $\lambda$ | growth rate parameter |
| $\lambda_C^2$ | $(c_S(T_{el}-T_0)/2\Lambda)(h_C/h)$ |
| $\Lambda$ | latent heat [J kg$^{-1}$] |
| $\nu$ | kinematic viscosity [m$^2$ s$^{-1}$] |
| $\rho$ | density [kg m$^{-3}$] |
| $\tau_C$ | $((C_S-C_X)/(C_S-C_I))(HL/D\,Sh)$ |
| $\tau_T$ | $\rho_L c_L HL/k_L\,Nu$. |

Subscripts

| | |
|---|---|
| $C$ | concentration |
| e | value at equilibrium |
| I | initial value |
| L | liquid |
| S | solid |
| $T$ | temperature |
| $X$ | interface |
| 0 | value at $x=0$ |
| $\infty$ | limit as $t\to\infty$. |

tion and measuring their density to six figure accuracy with a Paar DMA density meter. The average temperature and concentration of the liquid were calculated from the integrated profiles. Experiments were run for varying lengths of time and the crystal mass weighed and analyzed to find the average crystal wall thickness and composition as a function of time.

In finding the heat transfer from the liquid to the crystal interface it was necessary to allow for the heat gained from conduction through the polystyrene insulation and from cooling the plexiglass walls. The design of the tank was not ideal in that the thick plexiglass walls had considerable heat capacity.

For about the first half hour, the heat transfer to the solution was so high that the cold wall could not be maintained at a constant temperature. Since the boundary conditions then were unrepresentative, for comparison with the analysis the time was counted from 15 min (12 min for the shorter tank) after the actual start of the experiment. At this initial time $t_I$ it was assumed that the crystal thickness was zero and the temperature was the measured temperature in the tank.

### 3. EXPERIMENTAL RESULTS

Figure 3 is a schematic diagram of the system. The model deals with quantities which are averaged over height and so the diagram depicts one-dimensional solidification in a confined region of length $L$. The solid–liquid interface $X(t)$ advances in the $X$-direction from the 'contact' ($x=0$) which is held at a constant temperature, and as it does so the temperature $T_L$ and concentration $C_L$ of the liquid decrease. We are interested in the thickness of the crystals, the properties of the liquid and the conditions at the interface, $T_X$ and $C_X$ as a function of time.

Figure 4 shows a plot of $X(t)$. It is seen that crystal growth is very similar for both tank lengths and closely follows a power law

$$X \propto t^{0.625}. \tag{1}$$

Figure 5 shows that over most of the time of the experiment the average temperature and concentration of the solution fall approximately exponentially with time and that the time-scales are shorter for the shorter tank. The exponential behavior is not so apparent for the temperature of the shorter tank because of heat leakage, as will be discussed in Section 5. The lines give the fit of the analytical model.

In addition to these measured quantities, it is essential to know the conditions at the solid–liquid interface. In one experiment, $T_X$ was measured as a function of time and height by holding a thermistor against the crystal surface (Fig. 6). The thermal boundary layer, the crystal roughness and the thermistor bead were all about the same size (1–2 mm) so the scatter of the data is not remarkable and the results are probably a good indication of the temperature seen by the 'average' interface. The results from a thermistor which was held fixed as the crystals grew past it agrees well.

Once the tank became stratified, $T_X$ varied with height, however the average temperature was constant

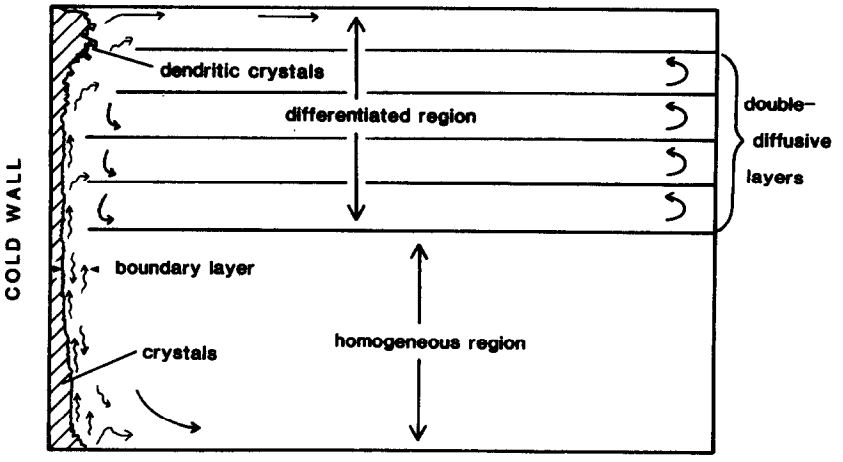


FIG. 1. Schematic diagram of typical side-crystallization experiment.

to within $\pm 0.5°C$, which is within the resolution of the measurements. Isolated values of the interface temperature taken in other experiments under different conditions are plotted as a function of initial liquid concentration in Fig. 7. The data run quasi-parallel to the saturation curve.

The forms of these curves will be explained in Section 5, after the development of the analytical model.

## 4. ANALYSIS

In this section a simple mathematical model of the system will be derived from the conservation laws of mass and heat. The model describes the evolution of the mean properties of the system—the temperature and concentration in the liquid and at the interface, and the quantity of crystallized solid. The key parameters *Sh* and *Nu* must be found experimentally.

The analysis is applied to the simplest case of a saturated solution in a semi-infinite region, and then the complications of superheat and a confined environment are added. First the results of the classical solidification problem are given for reference.

### 4.1. *The classical solidification problem*

The classical Stefan problem of a phase change boundary advancing into a semi-infinite melt

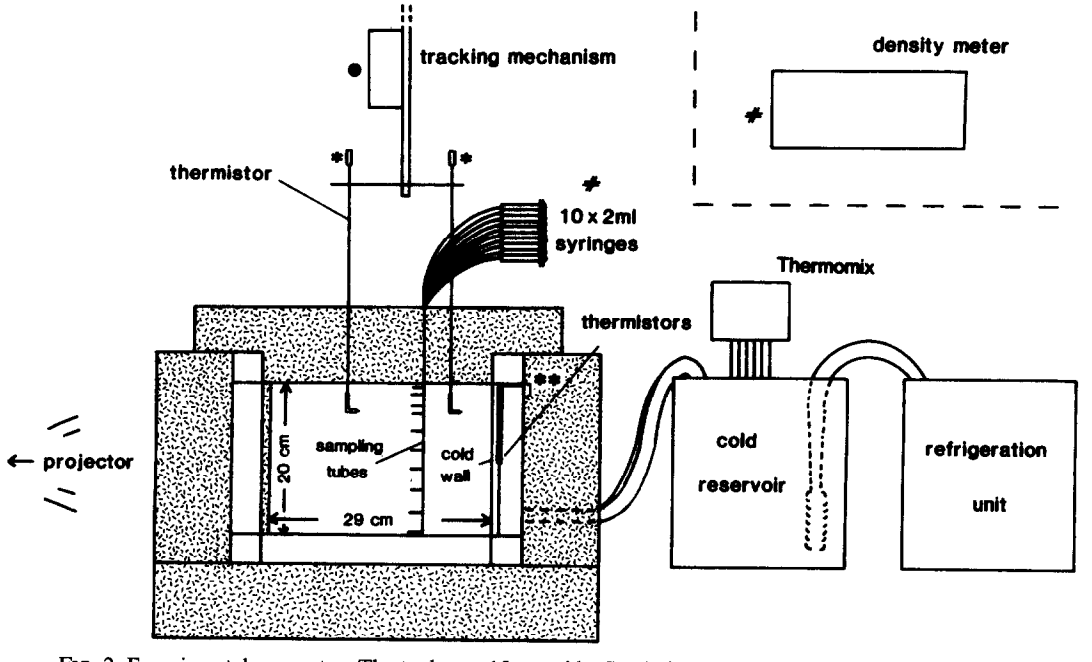


FIG. 2. Experimental apparatus. The tank was 15 cm wide. Symbols indicate connections between pieces of equipment.

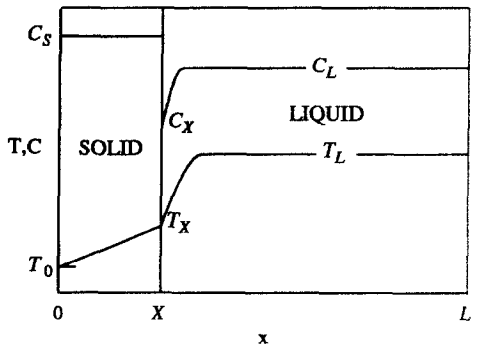


FIG. 3. Experimental system considered as a one-dimensional solidification problem.

($C_L = C_S$) from a constant temperature wall was solved by Neumann and is set out in ref. [8]. It is a one-dimensional heat conduction problem and $T_X$ is constant at the melting temperature.

Solving the thermal energy equations with the appropriate boundary conditions yields the temperature in the liquid and the solid as functions of time and position, $T_L(x, t)$, $T_S(x, t)$. The position of the interface is given by

$$X = 2\lambda(\kappa_S t)^{1/2} \tag{2}$$

where $\lambda$ is the growth rate parameter. For the special case of $T_X = T_1$ and for small values of $\lambda$

$$\lambda^2 = \frac{c_S(T_X - T_0)}{2\Lambda}. \tag{3}$$

The classical system evolves according to the inverse square root of time. The crystal growth rate (and hence the latent heat release) and the fluxes of sensible heat out of the liquid and the solid all vary as $t^{-1/2}$, and so the contributions to the total heat flux from these three sources remains in the same proportion.

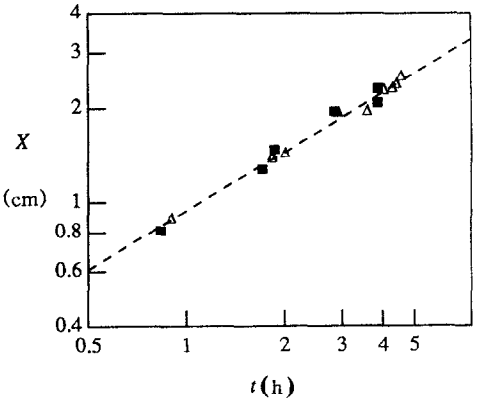


FIG. 4. The thickness $X$ of the solid as a function of time: △, $L = 29.4$ cm; ■, $L = 20$ cm. Dashed line $X = 0.94t^{0.625}$.

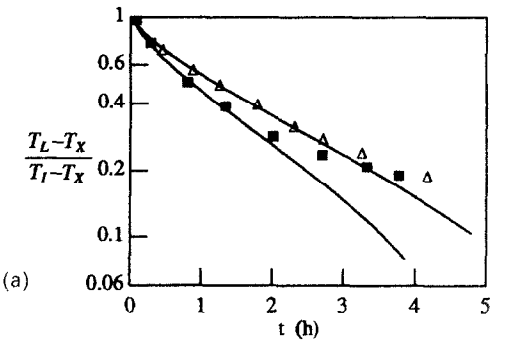


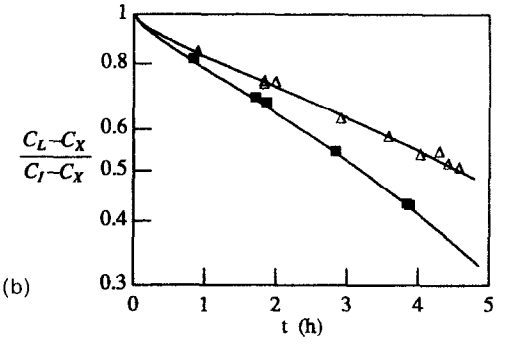


FIG. 5. The normalized temperature (a) and concentration (b) of the liquid as a function of time: △, $L = 29.4$ cm; ■, $L = 20$ cm; solid lines, theoretical solution. Normalization with respect to $t_1$ initial conditions and measured $\bar{T}_X$ for the longer tank. $\bar{T}_X$ for $L = 20$ cm was taken from the theoretical solution.

### 4.2. *The experimental system: the equations*

The experimental system differs from the one above in that: (1) the liquid is in a confined region; (2) transfer between the liquid and the interface is by convection rather than conduction; and (3) the liquid

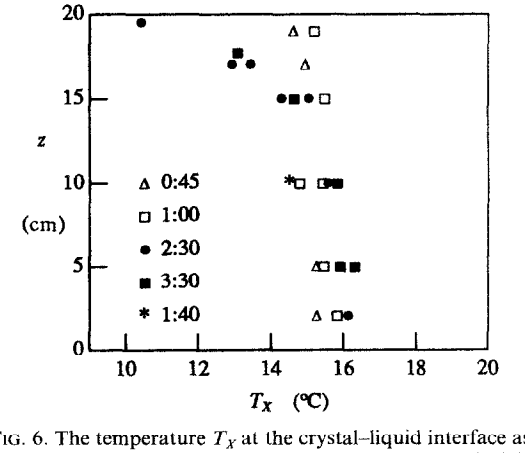


FIG. 6. The temperature $T_X$ at the crystal–liquid interface as a function of height at times indicated ($L = 29.4$ cm). * is the result from a fixed thermistor.

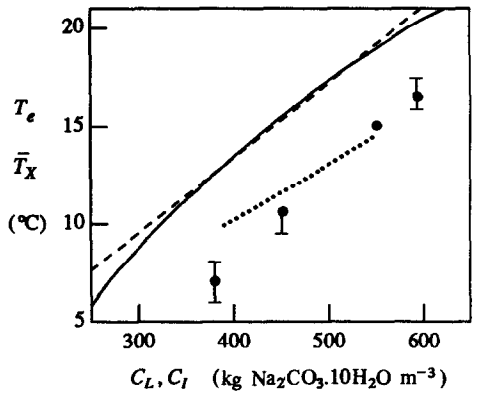


FIG. 7. The saturation curve for $Na_2CO_3$ over the range of experimental conditions. The dashed line is equation (10). The points are measured values of $T_X$, and the dotted line is the theoretical prediction of $\bar{T}_X$ as a function of $C_I$.

is a solution not a melt, so mass transfer as well as heat transfer limits the crystal growth.

For the classical problem there are three unknowns, $T_L(x, t)$, $T_S(x, t)$ and $X(t)$. In the experimental system, there are seven: $T_I(t)$, $T_S(t)$, $X(t)$, $C_I(t)$, $C_S(t)$, $T_X(t)$ and $C_X(t)$, which can be solved for using the following seven equations.

If the assumptions are made that the concentration of the solid is fixed and the temperature distribution through the layer of crystals is linear then

$$C_S = \text{constant} \tag{4}$$

$$T_S(x, t) = \frac{x(T_X - T_0)}{X(t)}. \tag{5}$$

The conservation laws for heat and mass, at the interface and within the confined region, respectively, can be written as

$$\Lambda\rho_S \frac{dX}{dt} = k_S \frac{T_X - T_0}{X} - k_L \left(\frac{T_L - T_X}{H}\right) Nu \tag{6}$$

$$(C_S - C_X)\frac{dX}{dt} = D\left(\frac{C_L - C_X}{H}\right) Sh \tag{7}$$

$$\rho_L c_L (L - X)\frac{dT_L}{dt} = -k_L \left(\frac{T_L - T_X}{H}\right) Nu \tag{8}$$

$$\left(\frac{C_S - C_X}{C_S - C_I}\right)\frac{(L-X)^2}{L}\frac{dC_L}{dt} = -D\left(\frac{C_L - C_X}{H}\right) Sh. \tag{9}$$

Finally, if the equilibrium (saturation) curve is approximated by a straight line

$$C_L \approx mT_e + b \tag{10}$$

then the assumption of equilibrium at the interface implies

$$C_X = mT_X + b. \tag{11}$$

Figure 7 shows the saturation curve for $Na_2CO_3$. Over the experimental range of concentrations ($C_L$ = 350–550) a good linear approximation is given by $m = 26$ and $b = 52$.

In the experiments $C_S$ changed only 3% over 2 h. $T_S$ would actually be curved, the difference in the thermal gradients at $x = 0$ and $X$ corresponding to the heat flux required to cool the growing solid. For the experimental conditions this flux was only 5% of the flux through the solid so the temperature gradient was almost linear. Strictly speaking, there must be some degree of supercooling at the interface (i.e. $C_X > C_e(T_X)$) for growth to occur, but in general this is unknown and very hard to determine. For the experiments it is likely to be small, so equation (11) is taken as a good approximation.

Eliminating $dX/dt$ from equation (6) with the use of equation (7), the expression for conservation of heat at the interface becomes

$$k_S \frac{T_X - T_0}{X} = \left(\frac{\Lambda\rho_S D}{C_S - C_X}\right)\left(\frac{C_L - C_X}{H}\right) Sh + k_L \left(\frac{T_L - T_X}{H}\right) Nu. \tag{12}$$

In this form it is clear that the heat conducted out of the system has its source in convective mass transfer and heat transfer, and that a balance is reached through the variation of the interface conditions.

The concentrations $C_L$ and $C_X$ can be eliminated from the equations using the linear relationship between concentration and equilibrium temperature, equations (10) and (11). Thus the seven equations are reduced to four, in terms of the temperatures $T_e$, $T_X$ and $T_L$ and the solid thickness $X$. Equations (12) and (7)–(9) become

$$\frac{T_X - T_0}{X} = h_C(T_e - T_X) + h_T(T_L - T_X) \tag{13}$$

$$\frac{dX}{dt} = \frac{2h\lambda_C^2\kappa_S}{T_{eI} - T_0}(T_e - T_X) \tag{14}$$

$$\frac{dT_L}{dt} = -\frac{1}{\tau_T}\left(\frac{L}{L-X}\right)(T_L - T_X) \tag{15}$$

$$\frac{dT_e}{dt} = -\frac{1}{\tau_C}\left(\frac{L}{L-X}\right)^2(T_e - T_X) \tag{16}$$

with initial conditions

$$X = 0, \quad T_e = T_{eI}, \quad T_L = T_{LI} \quad \text{at} \quad t = 0. \tag{17}$$

Some groups of variables have been combined into new parameters. The $h$'s are normalized convective heat transfer coefficients, $\lambda_C$ is a modified growth rate parameter, and the $\tau$'s are time-scales for change in the liquid. The $h$'s and $\tau$'s are time dependent through the variation of $C_S - C_X$, $Sh$ and $Nu$, however as a first approximation it will be assumed that they are constants.

Finally, the normalized equations (13)–(17) can be nondimensionalized using the scheme given in Table 1

Table 1. Dimensionless parameters in terms of normalized parameters and physical quantities

| Parameter | Normalization | Dimensional description |
|---|---|---|
| $\theta$ | $(T-T_0)/(T_{el}-T_0)$ | |
| $x$ | $hX$ | $[(\rho_S\Delta m/(C_S-C_X))D\,Sh+k_L\,Nu](X/k_SH)$ |
| $t^*$ | $2h^2\lambda_C^2\kappa_S t$ | $[(\rho_S\Delta m/(C_S-C_X))D\,Sh+k_L\,Nu][(C_I-C_0)/(C_S-C_X)](D\,Sh/k_SH^2)t$ |
| $h_C^*$ | $h_C/h$ | $[1+(k_L\,Nu/D\,Sh)((C_S-C_X)/\rho_S\Delta m)]^{-1}$ |
| $\gamma$ | $\tau_T/\tau_C$ | $(D\,Sh/\kappa_L\,Nu)[(C_S-C_I)/(C_S-C_X)]$ |
| $x_\tau$ | $2h^2\lambda_C^2\kappa_S\tau_C$ | $[(\rho_S\Delta m/(C_S-C_X))D\,Sh+k_L\,Nu][(C_I-C_0)/C_S-C_I)](L/k_SH)$ |
| $l$ | $hL$ | $[(\rho_S\Delta m/(C_S-C_X))D\,Sh+k_L\,Nu](L/k_SH)$ |
| $R$ | $(h_T/h)[(T_{el}-T_{LI})/(T_{el}-T_0)]$ | $[(T_{el}-T_{LI})/(T_{el}-T_0)][1+(D\,Sh/k_L\,Nu)(\rho_S\Delta m/(C_S-C_X))]^{-1}$ |

$$\frac{\theta_X}{x}=h_C^*(\theta_e-\theta_X)+h_T^*(\theta_I-\theta_X) \tag{18}$$

$$\dot{x}=\theta_e-\theta_X \tag{19}$$

$$\dot{\theta}_L=-\frac{1}{\gamma x_\tau}\left(\frac{l}{l-x}\right)(\theta_I-\theta_X) \tag{20}$$

$$\dot{\theta}_e=-\frac{1}{x_\tau}\left(\frac{l}{l-x}\right)^2(\theta_e-\theta_X) \tag{21}$$

$$x=0,\quad \theta_e=1,\quad \theta_L=1-\frac{R}{h_T^*},\quad \text{at}\quad t^*=0. \tag{22}$$

Differentiation is with respect to normalized time $t^*$. Equation (18) (cf. equation (12)) describes the heat balance at the interface between conduction (left-hand side) and convection, and equation (19) the growth rate of the crystal layer as a result of the mass transfer from the liquid. Equations (20) and (21) describe the rate of change of temperature and concentration in the confined liquid as a result of convective transfer to the solid–liquid interface. The complexity of the dimensional expressions in Table 1 is principally due to the complexity of $h$, which incorporates both thermal and compositional convective transfer.

### 4.3. *Semi-infinite liquid*

In an unconfined environment the temperature and concentration of the liquid, $\theta_L$ and $\theta_e$, are constants and equations (18) and (19) alone describe the system. If the liquid is saturated (i.e. $\theta_L=\theta_e$) then equation (18) becomes

$$\theta_X=\frac{x}{x+1} \tag{23}$$

so that the interface temperature $\theta_X$ varies from 0 to 1 (i.e. $T_X$ varies between $T_0$ and $T_e$) as $x$ increases. The crystal wall and the convective boundary layer can be seen as two thermal resistances in series. $x$, the ratio of $X$ and $1/h$, is a scaling of the crystal thickness which indicates the relative importance of conduction and convection.

Solving equations (18) and (19) gives

$$x=(1+2t^*)^{1/2}-1 \tag{24}$$

$$\theta_X=1-(1+2t^*)^{-1/2}. \tag{25}$$

At small values of $x$ ($\ll 1$) crystal growth is controlled by convective transport and the wall grows approximately linearly

$$x\approx t^*;\quad \theta_X\approx t^*. \tag{26a,b}$$

At large values of $x$ ($\gg 1$) the growth rate is controlled by conduction of heat through the wall and

$$x\approx(2t^*)^{1/2};\quad \theta_X\to 1 \tag{27a,b}$$

or

$$X\approx 2\lambda_C(\kappa_S t)^{1/2};\quad T_X\to T_e. \tag{28a,b}$$

Equation (28a) has the same form as Neumann's result equation (2) and the choice of the parameter name $\lambda_C$ becomes clear.

A plot of the normalized crystal thickness and interface temperature as a function of time is shown in Fig. 8(a), together with dimensional scales appropriate to the experimental conditions. It is seen that equations (26) are a good approximation for less than a minute, when the crystal thickness is less than 1 mm. A laboratory experiment of a few hours takes place mainly in the transition region between the two limits.

4.3.1. *Supercooled/heated semi-infinite liquid.* When the semi-infinite liquid is not on the saturation curve, equation (18) becomes

$$\theta_X=(1-R)\frac{x}{x+1} \tag{29}$$

where $R$ (Table 1) is the ratio of the transport rate of the excess sensible heat to the transport rate of the 'saturation' heat (sensible plus latent). If the liquid is supercooled $R$ is positive. Solving equation (29) with equation (19) gives

$$t^*=\frac{1}{R}\left[x+\left(1-\frac{1}{R}\right)\ln|1+Rx|\right] \tag{30}$$

$$\theta_X=|1-R|[1-(1+2t^*)^{-1/2}]. \tag{31}$$

At small $x$ ($\ll 1/|1-R|$) equation (26a) is recovered, but the interface temperature is modified because a different amount of sensible heat is supplied along with the latent heat

$$x\approx t^*;\quad \theta_X\approx|1-R|t^*. \tag{32a,b}$$

At later times ($x\gg|R-1|/R$) for positive $R$

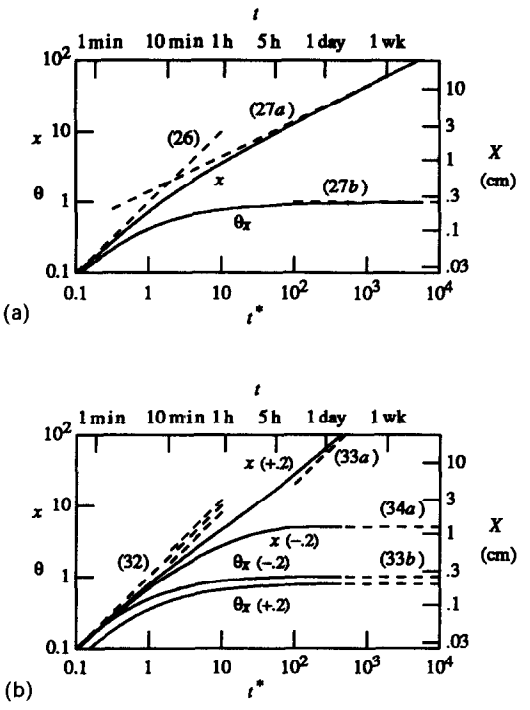


FIG. 8. Normalized interface position $x$ and temperature $\theta_X$ in a semi-infinite liquid: (a) saturated liquid; (b) superheated ($R = -0.2$) and supercooled ($R = 0.2$) liquid. Dimensional scales appropriate to the experimental system. Dashed lines are asymptotes given by indicated equations.

$$x \approx Rt^*; \quad \theta_X \to |1-R|. \tag{33a,b}$$

Again growth is linear because it is controlled by convective transport. The factor $R$ occurs because it is controlled by $h_T$ and the supercooling $T_e - T_L$ rather than by $h$ and $T_e - T_0$.

If the liquid is superheated ($R < 0$) then small time behavior is still described by equations (32), but as $t^* \to \infty$ a maximum value of $x$ is approached

$$x_\infty = \frac{1}{|R|}; \quad \theta_X \to 1 \tag{34a,b}$$

when the superheat supplied by thermal convection is exactly balanced by conduction through the solid. The existence of this maximum for the case of ice freezing in a semi-infinite environment was pointed out in ref. [9].

The behavior of the non-saturated system is illustrated in Fig. 8(b) for values of $R = 0.2$ and $-0.2$. For the experimental parameters this corresponds to a superheating/cooling of about 6°C. After a day the superheated system has produced its limiting crystal thickness of 12 mm. In the same time the saturated system forms four and the supercooled system 14 times as much solid.

### 4.4. *Confined liquid*

In a finite liquid $T_L$ and $T_e$ are variables, and the conditions at the interface vary according to changes in the environment as well as the changing thickness of solid.

The asymptotic state of the system is one of uniform temperature $T_0$, the liquid is saturated and the solid has a finite thickness

$$T_{X\infty}, T_{L\infty} = T_0, \qquad \theta_{X\infty}, \theta_{L\infty} = 0$$
$$C_{L\infty} = C_0, \quad \text{i.e.} \quad \theta_{e\infty} = 0$$
$$X_\infty = \left(\frac{C_I - C_0}{C_S - C_0}\right)L, \qquad x_\infty = \frac{l}{\theta_S}. \tag{35}$$

($\theta_S$ is an equivalent saturation temperature for the concentration of the solid $C_S$.) It is now of interest to investigate how the system approaches the asymptotic state.

Equations (18)–(22) can be reduced to

$$\gamma x_\tau (1+x)\ddot{x} + \gamma \frac{x_\tau}{x}\left\{1 - \frac{x}{x_\tau}\left(\frac{l}{l-x}\right)\left[1 - \frac{1}{\gamma}(1+h_C^* x)\right.\right.$$
$$\left.\left. -(1+h_T^*)x\frac{l}{l-x}\right] - \dot{x}\right\}\dot{x} - \frac{l}{l-x}\left[1 - \frac{x}{x_\tau}\left(\frac{l}{l-x}\right)\right] = 0 \tag{36}$$

$$x = 0, \quad \dot{x} = 1, \quad \ddot{x} = -\left[(1-R) + \frac{1}{x_\tau}\right] \quad \text{at} \quad t^* = 0. \tag{37}$$

This second-order non-linear differential equation was integrated numerically using Hamming's predictor–corrector method with starting values provided by a fourth-order Runge–Kutta.

The evolution of the system depends on five parameters (since $h_T^* = 1 - h_C^*$). $h_C^*$ is a measure of the relative importance of compositional and thermal convection in determining the conditions at the interface; $\gamma$ compares the effectiveness of thermal vs compositional convection in altering the properties of the liquid (it contains the heat capacity of the liquid which $h_C^*$ does not); $l$ gives the physical size of the system; $R$ is a measure of the initial supercooling; $x_\tau$ of the initial concentration of the solution. $x_\tau$ is the normalized time corresponding to $t = \tau_C$, the time-scale for change of liquid concentration. Similarly, $\gamma x_\tau$ corresponds to the time-scale $\tau_T$ for change of liquid temperature.

The combination of the five parameters allows for a rich variety of behavior as illustrated in Figs. 9(a)–(d). Common features follow from the boundary conditions of the problem. $x$ rises monotonically from zero and approaches a limiting value of $x_\infty$; $\theta_L$ and $\theta_e$, the temperature and saturation temperature (i.e. concentration) of the liquid, fall from their initial values to zero; the interface temperature $\theta_X$ rises from zero to a maximum value then falls again to zero.

The evolution of the system can be divided roughly into three regimes, as for the semi-infinite case.

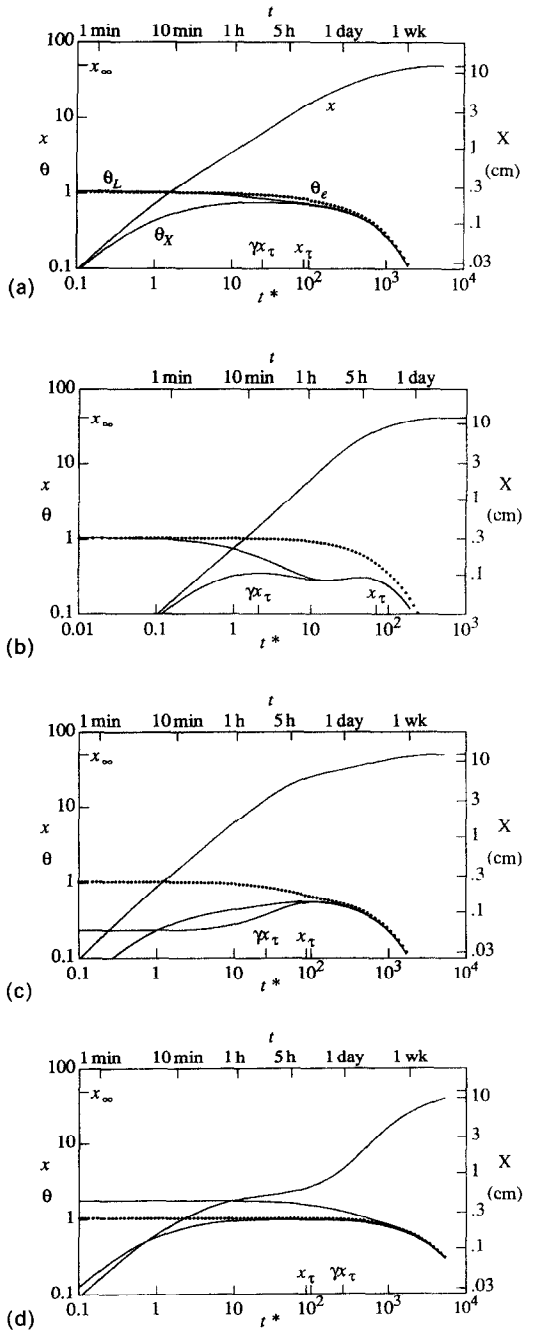


FIG. 9. Normalized crystal thickness $x$ and temperatures $\theta_e$ (dotted line), $\theta_L$ and $\theta_X$ in a confined region: (a) experimental system, $L = 29.4$ cm, $h_C^* = 0.35$, $\gamma = 0.3$, $x_\tau = 86$, $l = 116$, $R = -0.05$; (b) laminar convective transport ($Nu$, $Sh$ from equations (46)), $h_C^* = 0.05$, $\gamma = 0.03$, $x_\tau = 70$, $l = 100$, $R = -0.05$; (c) as for (a) with $R = 0.5$ (initial supercooling of 14°C); (d) as for (a) with $R = -0.5$ (initial superheating of 14°C) and $\gamma = 3$.

4.4.1. *Short-time behavior.* When $x$ is sufficiently small, $x$ and $\theta_X$ are given by equations (32), and $\theta_e$ and $\theta_L$ are approximately constant at their initial values. 'Small' $x$ is determined by the criterion $x \ll 1/|1-R|$ (i.e. convection limits growth) plus criteria that the conditions in the environment are not changing quickly, $x \ll l$, $x \ll x_\tau$ and $x \ll \gamma x_\tau$. It takes extreme values of the physical parameters, however, for the last three criteria to be important. For the experimental conditions it would require $L \ll 2$ mm, a solution 500 times as dilute, or a ratio of heat to mass transfer 300 times as great.

From Fig. 9 $x$ and $\theta_X$ increase linearly for $x < 0.1$. This corresponds to $X < 0.2$ mm and $t < 30$ s so there are no experimental observations of this growth region.

4.4.2. *Long-time behavior.* After long times compared with $x_\tau$ and $\gamma x_\tau$, the crystal thickness approaches $x_\infty$, and $\dot{x}$, $\theta_L$, $\theta_X$ and $\theta_e$ all decrease to zero exponentially with time-scale

$$\tau_\infty = \frac{x_\infty}{2}\left\{(1+h_C^* x_\infty)\frac{x_\infty}{x_\tau}+(1+h_T^* x_\infty)\gamma + \left[[(1+h_C^* x_\infty)\frac{x_\infty}{x_\tau}-(1+h_T^* x_\infty)\gamma]^2 + 4h_C^* h_T^* \frac{x_\infty^3}{x_\tau}\gamma\right]^{1/2}\right\}. \quad (38)$$

The starting values of the exponential decrease must however be found from numerical integration of the equations through the transitional region.

If conduction ultimately dominates transport (i.e. $h_C^* x_\infty$, $h_T^* x_\infty \gg 1$) this simplifies to

$$\tau_\infty = \frac{x_\infty^2}{x_\tau}[h_C^* x_\infty + h_T^* \gamma x_\tau]. \quad (39)$$

4.4.3. *Transitional time behavior.* Figure 9(a) was calculated using parameter values for the longer experimental tank as found in the next section. It is seen that the interface temperature $\theta_X$ reaches a maximum and then falls again, and in the transitional time period between a few minutes and several hours it varies little because the rising value of $x$ is compensated by the falling values of the temperature and concentration differences $(\theta_L - \theta_X)$ and $(\theta_e - \theta_X)$ (equation (18)).

The concentration $\theta_e$, the dotted curve, starts at a value of 1 (by definition) and decreases gradually to meet $\theta_X$. From equation (19), $\theta_e > \theta_X$ as long as the crystals are growing.

The liquid temperature $\theta_L$ starts with a value greater than 1 (slightly superheated) and falls, in a similar way to $\theta_e$, towards $\theta_X$. Comparing equations (20) and (21), as long as $\gamma$ and $\theta_{LI}$ are not too different from 1, we would expect similar behavior from $\theta_L$ and $\theta_e$. In the experiments $\gamma \approx 0.3$ and $\theta_{LI} < 1.1$. Because the time-scale ratio $\gamma < 1$, $\theta_L$ drops more quickly than $\theta_e$ and after several minutes the liquid becomes supercooled. This is an important point: in general we would expect $\gamma < 1$ because of the high value of $\kappa_L/D$, so in general we would expect systems to become supercooled.

The value of $x$ rises monotonically towards $x_\infty$. The slope $\dot{x}$ starts at 1 and asymptotically approaches

0, but in between it is influenced by the changing conditions in the interior. Figure 8(b) illustrates that in an infinite environment at long time the growth rate is determined by the supercooling. Analogously, crystal growth in the confined environment adjusts itself to the instantaneous supercooling. Substituting $\theta_X$ from equation (18) into equation (19)

$$\dot{x} = \frac{x}{1+x}\left[\frac{\theta_e}{x} + h_T^*(\theta_e - \theta_L)\right]. \tag{40}$$

Thus, for $x \gg 1$ the growth rate is more or less proportional to the supercooling.

The next three graphs illustrate the effect of varying the parameters. Figure 9(b) was generated using parameters appropriate to single component laminar convection on a flat wall. In this case $D \ll \kappa_L$ so that (Table 1) $h_C^* \ll 1$ and $\gamma \ll 1$—convective mass transfer is much slower than heat transfer—and the time-scales for change in the concentration and temperature in the liquid are widely separated.

The interface temperature $\theta_X$ (see equation (19)) depends on both compositional and thermal transfer. In this case, it is controlled first by one and then by the other. Over the time-scale $\gamma x_\tau$, changes in $\theta_X$ are primarily a balance between the rapid changes in liquid temperatures $\theta_L$ and changes in $x$. $\theta_X$ reaches a peak and falls off slowly as thermal transfer to the interface decreases. The large value of $h_T^*$ and the slow rate of change of $\theta_e$ allow $\theta_X$ to respond sensitively to changes in $\theta_L$. For $t^* \gg \gamma x_\tau$ and over the scale $x_\tau$, $\theta_X$ is determined by a balance between concentration $\theta_e$ and $x$. This occurs even though $h_C^*$ is very small, because $\theta_L - \theta_X$ is negligible. Note that the laminar transfer coefficients result in a greatly reduced crystal thickness and interface temperature, a faster change in $\theta_L$ and a slower change in $\theta_e$.

Figure 9(c) represents a highly supercooled system. The crystal growth rate is enhanced and the interface temperature depressed. The supercooling maintains the initially high growth rate for longer, this decreases concentration $\theta_e$ more quickly, and towards the end of the transitional period the growth rate is slower than for Fig. 9(a). Over most of the transitional period $\theta_X > \theta_L$ due to the release of latent heat so that the liquid is warmed rather than cooled from the interface.

The influence of superheat is illustrated in Fig. 9(d). As we would expect from Fig. 8(b), $\theta_X$ is increased and the growth rate of the crystals is depressed. In this example the ratio of time-scales $\gamma > 1$, and so the system does not become supercooled. However, over the time-scale $\gamma x_\tau$ the superheat does decrease and the crystal growth rate then abruptly increases.

Varying $l$ (not illustrated in the graphs) changes the distance scales and $x_\tau$ influences both distance and time-scales. The asymptotic thickness of the solid depends on the concentration and reservoir length

$$x_\infty = \frac{x_\tau l}{x_\tau + l}. \tag{41}$$

Increasing $x_\tau$ expands the transitional region, and decreasing it to $O(1)$ makes the transitional region very small so that convection dominates until crystallization is almost complete.

## 5. THEORY VS EXPERIMENT

The agreement between theory and experiment is very good, as shown by a comparison of the data points and the theoretical curves in Figs. 4–6. The trends in the data observed in Section 3 were as follows. $T_X$ was roughly constant; after an initial faster decrease, $T_L$ and $C_L$ fell exponentially to the conditions at the interface, with shorter time-scales for the shorter tank length; $X$ grew as a power law, with similar values for the two tank lengths. Figure 7 suggests that $T_X$ as a function of the initial concentration, runs subparallel to the saturation curve.

To explain these trends, we first observe that $\bar{T}_X$ was roughly constant between the recorded times of 30 min and $3\frac{1}{4}$ h. During this time the crystals grew about 1.5 cm, a small fraction of the tank length $L$ (29 cm). If, then, the approximations are made that

$$T_X = \text{constant}, \quad \frac{L}{L-X} \approx 1$$

then equations (15) and (16) have the solutions

$$T_L - T_X = (T_{LI} - T_X)\, e^{-t/\tau_T} \tag{42}$$

$$T_e - T_X = (T_{eI} - T_X)\, e^{-t/\tau_C} \tag{43}$$

so that the temperature and concentration of the liquid do fall exponentially to the interface conditions. The thermal and compositional time-scales $\tau_T$ and $\tau_C$ are proportional to $L$, fitting the observation of shorter time-scales for the shorter tank length.

Substituting equation (43) into equation (14)

$$X \approx \left(\frac{T_{eI} - T_X}{T_S - T_{eI}}\right) L(1 - e^{-t/\tau_C}). \tag{44}$$

Expanding out the exponential, the terms in $L$ cancel. To a first approximation $X$ is independent of $L$, accounting for the similarity of the curves in Fig. 4.

The power law behavior is fortuitous. $X$ is influenced in opposite directions by the falling liquid temperature and the falling concentration. For the parameter values of Fig. 9(a) the resulting curve happens to fit a power law, however, as Fig. 9(d) indicates, this is not the case for all parameter values.

The data in Fig. 7 suggest that $\bar{T}_X$ as a function of the initial concentration runs subparallel to the saturation curve, whereas the analytical model predicts that $\bar{T}_X$ should approach the saturation curve at lower $C_I$. The data, being isolated measurements at isolated heights instead of average values, are not sufficiently accurate to contest with the model. If more accurate data supported this trend, it would indicate that $h$ is a function of $C_I$.

5.1. *Sh and Nu*

The transfer coefficients of heat and concentration in two-component boundary layers at a rough surface are not in general known—they must be determined experimentally. Equations (42) and (43) show that if $T_\lambda$ is known, they can be determined from the time-scales $\tau_I$ and $\tau_C$. The slopes of the lines in Fig. 5 between $\frac{1}{2}$ and $3\frac{1}{4}$ h give values of

$$Nu \approx 65 \pm 6; \quad Sh \approx 6200 \pm 1600. \tag{45}$$

The errors given are due to a 25% uncertainty in the diffusivity $D$ ($4 \pm 1 \times 10^{-10}$ m$^2$ s$^{-1}$) and 5% uncertainties in the interface temperature and in the measurement of time-scales $\tau$. This can be compared with what would be expected for single component (i.e. only heat or composition) laminar boundary layers on a smooth stationary wall with the same boundary conditions [10]

$$Nu = 0.670 Ra_H^{1/4} \approx 82 \tag{46a}$$

$$Sh = 0.670 Rs_H^{1/4} \approx 800. \tag{46b}$$

The measured $Sh$ is 6–10 times greater than the value for a flat wall and the measured $Nu$ about 20% less.

The Sherwood number could be enhanced by three processes which affect the boundary layer structure—turbulence, the counter-flowing thermal boundary layer, and the three-dimensional roughness of the surface.

For free convection on a flat wall the critical Rayleigh number for the onset of turbulence is

$$Ra_c \approx 10^9 Pr^n \tag{47}$$

where estimates of the exponent $n$ vary from 0.5 to 2.5 [6]. For the laboratory conditions ($Sc \approx 4 \times 10^3$, $Rs \approx 5 \times 10^{12}$) the compositional boundary layer is laminar if $n > 1$. Surface roughness could decrease the transition value, but probably less than a factor of 2 [10]. The presence of the destabilizing thermal boundary layer might have a similar effect [11]. Direct observation of the boundary layer confirms that flow, though unsteady, is at most transitional.

In the experiments the surface roughness is an order of magnitude greater than the boundary layer thickness due to compositional diffusion. It influences transport firstly by increasing the surface area of the crystal liquid interface and also by changing the flow structure in the boundary layer.

The enhancement of mass transport at rough surfaces is a recognized, if not resolved, phenomenon in forced flows [10]. Increases in $Sh$ by a factor of 4 have been observed for turbulent flow through pipes [12–14], and up to a factor of 7.5 for rough particles in a packed absorber bed [15]. A central problem is a characterization of the roughness which will allow correlation with transport rates.

For pipe flow with similar, regular, two-dimensional grooves perpendicular to the flow [12], there was no mass transport enhancement for laminar flow. For turbulent flow, the maximum enhancement was independent of the roughness height $e$ and occurred when the roughness elements penetrated to the turbulent core. The enhancement was three times that due solely to the surface area, and thus primarily due to a change in the boundary layer flow field. For geometrically dissimilar sets of grooves [13], there was a variation in the maximum enhancement which correlated inversely with the ratio of pitch to height $p/e$ of the grooves. It is argued here that this can be largely explained by the variation of the surface area, which is proportional to $1 + ce/p$ where the geometrical factor $c$ is of the order of 1. This interpretation is supported by the fact that the enhancement was greater for larger $Sc$, when the compositional boundary layer was thinner relative to $e$.

In free convection the driving force is within the boundary layer itself, and so the geometry of the surface is still more intimately connected with the mass transport process. There has been very little work in this area, presumably because of lack of engineering applications. With the same equipment as the present experiments, an investigation of different surface textures [16] revealed a systematic change in the boundary layer structure with surface roughness, but no observable correlation of the mass transfer enhancement, which was between 4 and 13.

Because of the low turbulence in the boundary layer and its thinnest relative to the surface roughness, it is concluded that the principal reason for this higher $Sh$ is probably the increased surface area of the rough wall, which allows a larger number of sites for crystal growth. Undoubtedly the three-dimensional unsteady nature of the boundary layer flow also plays a role. If the increased mass flux is directly related to the surface area, $Sh$ may increase with time as the wall roughness increases, but the data are insufficient to test this.

With reference to $Nu$, the cold thermal boundary layer in the experiments is actually flowing upwards and its structure will be to a large extent determined by the driving compositional buoyancy. In other words, $Nu$ will not be determined by $Ra^{1/4}$ but will be some function of $Rs$, $Le$ and the buoyancy ratio $\Gamma$. That the heat transfer is similar to that predicted for a flat wall is reasonable since the boundary layer thicknesses (determined in the experiments by the roughness of the wall) would be similar.

5.2. *Initial conditions*

In order to compare the model with the data, it is necessary to determine $Sh$ and $Nu$ (as above) and the initial conditions $T_{LI}$ and $C_I$. Since we require $X = 0$ at $t = 0$, the effective $C_I$ is simply the initial concentration of the liquid. The corresponding $T_{LI}$ is not as obvious because, as described in Section 2, the experimental boundary conditions were not ideal in the first half hour. The value of $T_{LI}$ should be somewhere between the actual starting temperature of the liquid and the temperature after half an hour.

The best fit with the data was found by taking $T_{LI}$ equal to the temperature at $t_1$, half way between the

actual start and when the constant boundary temperature was achieved. That the best fit $T_{LI}$'s are physically reasonable values, supports the model.

The temperature data are not fitted as well as the concentration data because of the time-dependent heat leakage into the system, which was allowed for only crudely by assuming a higher effective specific heat for the liquid. The heat leakage was particularly serious for the short tank. After 3 h it was 50% and after 4 h 80% as great as the sensible heat flux through the crystals.

## 6. SUMMARY AND CONCLUSION

In this paper is presented a model of a binary liquid crystallizing at a constant temperature boundary from semi-infinite or confined environments. Heat and mass transfer between the solid and the liquid are by convection. The model aims to describe experimental systems where solutes crystallize out of aqueous solutions. Often such experiments are designed as dynamic analogies of more complex systems such as magmas or alloys. By providing an analytical description of the experimental system, the extent of the analogy and its limitations become more apparent.

The model is one-dimensional. It assumes that only one component crystallizes, the crystal–liquid interface is at equilibrium, the convective transfer coefficients are constant, and the solubility curve is linear. Four conservation equations for heat and mass are solved to find the evolving properties of the system.

In a semi-infinite environment there are two asymptotic states (Fig. 8). At short time evolution is controlled by convection and the crystal thickness and interface temperature change linearly with time. At long time for a saturated solution growth is limited by heat conduction through the crystals: the interface temperature approaches that of the liquid and the crystal wall grows as the square root of time. For a superheated or supercooled liquid, long-time growth is controlled by convection, this time of the superheat.

In a confined environment (Fig. 9) the short-time regime is the same as for an unconfined liquid. The long-time regime occurs when crystallization is almost complete and the conditions in the system exponentially approach the asymptotic state of uniform temperature. Transitional between the two regimes is a third, where there is an interaction between the growing crystal wall and the changing properties of the liquid. The model predicts that the interface temperature reaches a maximum and may remain approximately constant for a significant period of time. During this time the conditions in the liquid, to a first approximation, exponentially approach those at the interface.

There are two time-scales in this transitional regime, one for the change in the temperature and the other for the change in the concentration of the liquid. They are given by the ratio of the heat or 'concentration' capacity of the liquid to the convective heat or mass transfer rate at the interface. If the time-scales are very short then the transitional regime may be effectively eliminated; if they are very different in magnitude then evolution may be controlled first by one and then the other (Fig. 9(b)). An initial large degree of superheat can have a significant influence in the transitional regime (Figs. 9(c) and (d)).

Data from experiments, where a confined solution was cooled and crystallized from a side wall, agree very well with the predictions of the model and allow the evaluation of hitherto unknown quantities, the heat and mass transfer coefficients from a rough, vertical, advancing interface.

The assumptions of constant transfer coefficients, a linear solubility curve and equilibrium at the interface could easily be relaxed within the framework of the model. In the present case, the precision of the data does not warrant this. The most serious simplification of the model is that it is one-dimensional, so that it does not predict the form of the differentiation nor allow for the influence of the differentiated liquid on the crystallizing boundary.

The geometry of the confined region has an important influence on the nature and strength of convective transport. Crystallization of a heavy component at an upper boundary or a light component from a lower boundary will not drive convection and Newton's cooling law approach taken in this paper is inappropriate. See ref. [17] for an analysis of this geometry.

The opposite situation of the crystallization of a heavy component from a bottom boundary will drive compositional convection and may be expected to give good agreement with the model if the convective stirring is complete. However, bottom crystallization can lead to stratification of the liquid so that the fluid in contact with the crystallizing boundary is not representative of the average. Although crystallization at a side boundary will always generate a stratified liquid, integrated over the height of the wall the average interface is indeed in contact with the average liquid conditions and therefore good agreement with the one-dimensional model is not unexpected.

The present model is not presented as a realistic description of a magma chamber, however, two important relevant points emerge from this study. The first is the experimental observation of a mass transfer rate from a rough interface that is an order of magnitude greater than that from a flat wall. This should be considered when calculations are made of differentiation rates of magmas.

The other point is that a shorter time-scale for temperature compared to concentration change in the liquid—particularly likely if cooling takes place at a vertical or sloping boundary—will lead to supercooling of the liquid. This may encourage more dendritic or porous walls, crystallization in the interior of the magma chamber away from the walls, and will certainly act to quickly destroy any superheat a magma may have on emplacement.

*Acknowledgements*—I would like to thank Derek Corrigan and Joe Micaleff for the design and construction of the heat exchanger tank. I also gratefully acknowledge encouragement and useful discussions with Professor Stewart Turner and others at the Research School of Earth Sciences, Australian National University.

## REFERENCES

1. J. S. Turner, A fluid dynamical model of differentiation and layering in magma chambers, *Nature* **285**, 213–215 (1980).
2. A. R. McBirney, Mixing and unmixing of magmas, *J. Volcan. Geotherm. Res.* **7**, 357–371 (1980).
3. D. J. Hebditch, Contribution concerning the solidification problem. In *Moving Boundary Problems in Heat Flow and Diffusion* (Edited by J. R. Ockendon and W. R. Hodgkins). Clarendon Press, Oxford (1975).
4. C. F. Chen and J. S. Turner, Crystallization in a double-diffusive system, *J. Geophys. Res.* **85**, 2573–2593 (1980).
5. R. H. Nilson and M. R. Baer, Double-diffusive counter buoyant boundary layers in laminar natural convection, *Int. J. Heat Mass Transfer* **25**, 285–287 (1982).
6. R. H. Nilson, A. R. McBirney and B. H. Baker, Liquid fractionation. Part II: fluid dynamics and quantitative implications for magmatic systems, *J. Volcan. Geotherm. Res.* **24**, 25–54 (1985).
7. R. H. Nilson, Countercurrent convection in a double-diffusive boundary layer, *J. Fluid Mech.* **160**, 181–210 (1985).
8. H. S. Carslaw and J. C. Jaeger, *Heat Conduction in Solids* (2nd Edn). Clarendon Press, Oxford (1959).
9. C. A. Lapadula and W. K. Mueller, The effect of buoyancy on the formation of a solid deposit freezing onto a vertical surface, *Int. J. Heat Mass Transfer* **13**, 13–26 (1970).
10. H. Schlichting, *Boundary Layer Theory*. McGraw-Hill, New York (1979).
11. E. G. Josberger and S. Martin, A laboratory and theoretical study of the boundary layer adjacent to a vertical melting ice wall in salt water, *J. Fluid Mech.* **111**, 439–473 (1981).
12. D. A. Dawson and O. Trass, Mass transfer at rough surfaces, *Int. J. Heat Mass Transfer* **15**, 1317–1336 (1972).
13. S. Tantirige and O. Trass, Mass transfer at geometrically dissimilar rough surfaces, *Can. J. Chem. Engng* **62**, 490–496 (1984).
14. R. E. Acosta, R. H. Muller and C. W. Tobias, Transport processes in narrow (capillary) channels, *A.I.Ch.E. Jl* **31**, 473–482 (1985).
15. B. D. Young and B. M. van Vliet, The effect of surface roughness on fluid-to-particle mass transfer in a packed adsorber bed, *Int. J. Heat Mass Transfer* **31**, 27–34 (1988).
16. A. M. Leitch, Various aqueous solutions crystallizing from the side. In *Structure and Dynamics of Partially Solidified Systems* (Edited by D. E. Loper). NATO ASI Series E, No. 125. Nijhoff, Dordrecht (1987).
17. M. G. Worster, Solidification of an alloy from a cooled boundary, *J. Fluid Mech.* **167**, 481–501 (1986).

## EVOLUTION DE LA CRISTALLISATION D'UN SYSTEME BINAIRE DANS UNE REGION CONFINEE

**Résumé**—L'évolution dans le temps des propriétés moyennes d'un système binaire est étudiée pendant la cristallisation d'un composant sur une frontière à température constante pour un liquide soit semi-infini, soit confiné. Sont identifiés des régimes où l'évolution est contrôlée par le transport convectif dans le liquide, la conduction de chaleur à travers le cristal ou par les resources limitées du système confiné. Pour un liquide confiné il y a différentes échelles de temps pour le changement de température et de concentration. Il y a un bon accord entre les prédictions du calcul et les résultats des expériences quand une solution aqueuse binaire cristallise sur une frontière. Le nombre de Sherwood déterminé expérimentalement est, en ordre de grandeur, plus grand que pour la convection laminaire sur une paroi plane, et ceci est attribué à la rugosité de l'interface du cristal.

## ENTWICKLUNG DER KRISTALLISATION IN EINEM RÄUMLICH BEGRENZTEN BINÄREN SYSTEM

**Zusammenfassung**—Die zeitliche Entwicklung des Verhaltens eines binären Systems wird untersucht, wobei eine Komponente an einer Grenze konstanter Temperatur in einer entweder halbunendlichen oder begrenzten Flüssigkeit kristallisiert. Es werden Bereiche festgestellt, in denen die Entwicklung durch den konvektiven Transport aus der Flüssigkeit geprägt wird, solche mit Wärmeleitung im Kristall als Begrenzung oder solche mit begrenztem Zufluß in einem begrenzten System. Bei einer begrenzten Flüssigkeit gibt es verschiedene Zeitskalen für Temperatur- und Konzentrationsänderungen. Es zeigt sich eine gute Übereinstimmung zwischen Rechnung und Messung bei der Kristallisation einer binären wäßrigen Lösung an einer seitlichen Begrenzung. Die experimentell bestimmte Sherwood-Zahl ist um eine Größenordnung höher als die bei laminarer Konvektion an einer ebenen Wand, dies wird der Rauhigkeit der Kristall-Grenzschicht zugeschrieben.

## КРИСТАЛЛИЗАЦИЯ БИНАРНОЙ СИСТЕМЫ В ОГРАНИЧЕННОЙ ОБЛАСТИ

**Аннотация**—Исследуется изменение во времени средних свойств бинарной системы в случае кристаллизации одного компонента в полубесконечной или ограниченной области, заполненной жидкостью, при постоянной температуре на границе. Установлены режимы, при которых процесс определяется конвективным переносом в чидкости, теплопроводностью через кристаллы или лимитируется ограниченностью системы. В случае ограниченной области изменению температуры и концентрации соответствуют различные временные масштабы. Расчеты хорошо согласуются с результатами экспериментов, в которых бинарный водный раствор кристаллизуется у боковой границы. Экспериментально найденное число Шервуда на порядок больше, чем при ламинарной конвекции от плоской стенки, что объясняется шероховатостью межфазной границы кристалла.